AGU PUBLICATIONS

JGR

Journal of Geophysical Research: Planets

RESEARCH ARTICLE
10.1002/2017JE005271

Key Points:
- Model mid-infrared emissivity spectra of enstatite in different particulate sizes
- Explore the effectiveness of radiative transfer and T-matrix hybrid models
- Radiative transfer and T-matrix hybrid models are better suited for very fine particulates

Correspondence to:
G. Ito,
gen.ito@stonybrook.edu

Citation:
Ito, G., J. A. Arnold, and T. D. Glotch (2017), T-matrix and radiative transfer hybrid models for densely packed particulates at mid-infrared wavelengths, *J. Geophys. Res. Planets*, *122*, 822–838, doi:10.1002/2017JE005271.

Received 18 JAN 2017
Accepted 11 APR 2017
Accepted article online 18 APR 2017
Published online 4 MAY 2017

T-matrix and radiative transfer hybrid models for densely packed particulates at mid-infrared wavelengths

G. Ito[1], J. A. Arnold[2], and T. D. Glotch[1]

[1]Department of Geosciences, Stony Brook University, Stony Brook, New York, USA, [2]Department of Atmospheric, Oceanic and Planetary Physics, University of Oxford, Oxford, UK

Abstract Mid-infrared spectroscopy is a useful tool for remotely sensing the composition of Earth and other planets. Quantitative mineralogical investigations are possible using remotely sensed data; however, the difficulty in modeling complex interactions of light with particles that are on the order of the wavelength limits the usefulness of the remote sensing data. As part of an effort to develop a more effective treatment of light scattering in planetary regolith, we explore the ability of T-matrix and radiative transfer (RT) hybrid models to produce emissivity spectra that are consistent with laboratory measurements. Parameters obtained from T-matrix calculations are used in three different RT models to construct emissivity spectra of enstatite particles of different sizes. Compared to the widely used Mie/RT hybrid models, the T-matrix/RT hybrid models produce more consistent emissivity spectra for the finest particle size fraction (3.3 μm). Overall, T-matrix hybrid models produce improved emissivity spectra, but larger particle sizes are still difficult to model. The improvement observed in T-matrix/RT hybrid models is a result of the inclusion of multiple scattering in closely packed media, and it demonstrates the importance of the implementation of physically realistic factors in developing a more effective light scattering model for planetary regolith. Further development and implementation of this and similar hybrid models will result in an improvement in quantitative assessments of planetary particulate surfaces from mid-infrared spectra.

Plain Language Summary Remote sensing in the mid-infrared wavelengths (~5 - 50 μm) has been used widely to interpret the mineralogy of planetary surfaces. This technique works well when the material (soil, sand, rock, etc.) of interest is large compared to the reflected or emitted wavelength, however interpretation of such data is complicated by the presence of fine materials with sizes similar to or less than the wavelength of light. In these cases, a substantial portion of light is diffracted and accurate interpretations of mineralogy from remote sensing data becomes very difficult. This has been a problem as planetary surfaces are often covered with fine regolith - closely packed particles with sizes frequently on the order of mid-infrared wavelengths. In an effort to resolve this problem, one area of on-going research is the modeling of the interaction of light with such particles using light scattering models. We contribute to this effort by investigating advanced light scattering models that more realistically incorporate the physical conditions of planetary regoliths. We demonstrate that our approach achieves improvements that have been mostly unattainable with previous methods as well as give a critical analysis of its effectiveness. This work advances the development of more effective light scattering models for planetary regoliths which is crucial for accurate mineralogical analyses from remote sensing data.

1. Introduction

In remote sensing, mid-infrared (MIR) emission spectroscopy is useful for quantitative analysis of bulk silicate mineralogy, but complications exist that can limit this utility. These complications are mainly caused by the dependence of emissivity spectra on physical properties such as particle size, shape, and packing density [*Hunt and Logan*, 1972; *Salisbury and Eastes*, 1985; *Salisbury and Wald*, 1992]. For coarse particles (diameter much greater than the wavelength of light), emissivity spectra add linearly. However, when particle size is on the order of the wavelength of observed radiation, particle size and packing density variations lead to strong nonlinearity.

Works in the past have attempted to capture the nonlinear behavior by building light scattering models [*Conel*, 1969; *Wald*, 1994; *Moersch and Christensen*, 1995; *Wald and Salisbury*, 1995; *Mustard and Hays*, 1997; *Pitman et al.*, 2005; *Cheng et al.*, 2010]. In these works, the complex scattering of light by closely packed particles that are on the order of the wavelength of observed radiation are modeled using a combination of two

theories: Mie theory and the theory of radiative transfer (RT). While some success has been achieved using these methods, the computed spectra using these models do not completely agree with laboratory spectra. For example, in *Moersch and Christensen* [1995], root mean square error value of a fit between a laboratory and modeled emissivity of 15 μm sized quartz particles was 0.209 at 14.3–16.7 μm range where root mean square error above 0.1 is considered to be a poor agreement (reported in *Pitman et al.* [2005]). Moreover, these works have illustrated the complexity of modeling the physics of light scattering at wavelengths on the order of particle size. These models often invoke a large number of simplifying assumptions and physical parameters.

The work presented here expands on the ideas incorporated in previous light scattering models of regolith and further introduces a different technique, the T-matrix method, which has been used with some success to reproduce the effects of surface roughness and fine particulate mineral mixing in MIR spectra [*Hardgrove et al.*, 2016; *Glotch et al.*, 2016]. The T-matrix method, first presented by *Waterman* [1969] and later developed by different authors [*Mishchenko and Martin*, 2013], is based on explicit calculation of Maxwell's equations for densely packed particles, which avoids some of the assumptions inherent in the previous methods based on Mie theory [*Mishchenko*, 2008]. Previous studies based on Mie theory qualitatively captured the effect of particle size on MIR spectra, but the quality of Mie/RT modeled spectra was not acceptable for applications to planetary regolith studies due to significant errors between modeled and laboratory spectra. In order to make useful interpretations of a particulate planetary surface from MIR spectra, more accurate models are needed. T-matrix/RT hybrid models have shown initial, promising results (e.g., *Pitman et al.* [2015], *Glotch et al.* [2016]), and here, we closely examine the usefulness of T-matrix/RT hybrid models by computing MIR emissivity spectra of closely packed particles with sizes on the order of the wavelength.

2. Theories

2.1. Mie Theory

Mie theory is generally useful for studying the scattering of light by particles that are on the order of the wavelength of observed radiation. However, Mie theory is a single-scattering theory that assumes that the particles are well separated. The separation between particles must be approximately three times the particle radius [*van de Hulst*, 1957] for Mie theory to accurately predict particulate scattering. For planetary regolith, this assumption is not met and thus leads to inadequacies in Mie-based scattering models. Nevertheless, previous works have used Mie theory to study the scattering properties of planetary regolith as until recently this was the most computationally feasible available method, and to some extent, they have achieved reasonable results [*Conel*, 1969; *Wald*, 1994; *Moersch and Christensen*, 1995; *Wald and Salisbury*, 1995; *Mustard and Hays*, 1997; *Pitman et al.*, 2005]. However, it is now possible to implement more computationally intensive methods over enough wavelengths to approach laboratory spectral resolution.

2.2. T-Matrix Method

The T-matrix method, like Mie theory, can be used to compute scattering parameters for particulate media. Unlike Mie theory, the T-matrix method is applicable to a medium composed of closely packed particles as multiple scattering is incorporated. Its formulation is briefly reviewed here, and the reader is referred to some of the example references for more details [*Mackowski*, 1994; *Mackowski and Mishchenko*, 1996, 2011a, 2011b].

The formulation of the T-matrix method used in this work is essentially an extension of Mie theory, applied to a multiple sphere system, in a way that the goal is to determine the scattering coefficients for each sphere in a system. The electromagnetic field external to the spheres is a superposition of incident and scattered fields from all spheres. That is,

$$\boldsymbol{E}_{\text{ext}} = \boldsymbol{E}_{\text{inc}} + \boldsymbol{E}_{\text{sca}} = \boldsymbol{E}_{\text{inc}} + \sum_{i=1}^{N_S} \boldsymbol{E}_{\boldsymbol{sca},i} \tag{1}$$

where $\boldsymbol{E}_{\text{ext}}$, $\boldsymbol{E}_{\text{inc}}$, and $\boldsymbol{E}_{\text{sca}}$ are external, incident, and scattered fields, respectively. The system is composed of N_S spheres, and each sphere is indexed as the ith sphere. The incident and scattered fields are expressed as two different spherical harmonic functions. The vector spherical wave function (VSWF) expansions allow

a plane wave to be expressed as a superposition of spherical waves. This is useful for solving for the scattering properties of targets with spherical symmetry. Then, an application of the addition theorem and the boundary conditions to the incident and scattered VSWF expanded field equations reveals a linear relationship among the scattering coefficients of the spheres. This allows a creation of a system of equations that relates the scattered and incident field coefficients. The incident field is controlled, and thus, its coefficients are known, so a transition matrix, T, can convert the incident field coefficients into scattered field coefficients as

$$a^i_{mnp} = \sum_{j=1}^{N_s} \sum_{l=1}^{L_i} \sum_{k=-l}^{l} \sum_{q=1}^{2} T^{ij}_{mnpklq} p^j_{klq} \tag{2}$$

where p^j_{klq} and a^i_{mnp} represent incident and scattered field coefficients, respectively. Finally, the T matrix for the single, whole cluster, which contains information from all spheres, is determined by combining incident and scattered field coefficients that have been translated from the sphere centers to the cluster center.

The above formulation of the T-matrix solution briefly illustrates how a particle can interact with an electromagnetic field that has already interacted with another, or many other, particle(s) in addition to an incident field, whereas the Mie solution only allows an interaction of a particle with an incident electromagnetic field. The ability of the T-matrix method to allow electromagnetic interaction of one particle with many others forms the basis of multiple scattering that is essential to consider when modeling light scattering by densely packed particulates like planetary regolith.

2.3. Radiative Transfer Models

This work utilizes some of the simplest RT models based on two-stream approximation that have been frequently applied in planetary surface remote sensing studies. The two-stream approximation analytically solves the RT equation by finding the effective upward and downward intensities from a medium. The advantage of using these RT models is that they are computationally simple and accuracies are acceptable when calculating average intensities for densely packed, optically thick media [*Pitman et al.*, 2005]. Additionally, they are directly comparable to past works (e.g., *Moersch and Christensen* [1995]), and thus, we can more fairly assess the potential improvements from T-matrix/RT hybrid models. The simpler RT models will also serve as one of the foundations in developing other methods based on more complex RT models.

2.3.1. Conel Model

Parameters calculated using the Mie and T-matrix methods are input into RT models to calculate emissivity. *Conel* [1969] describes how spectral radiance traveling in a particular direction changes as it propagates through a medium, according to

$$\cos\theta \frac{\mathrm{d}I_\nu}{\mathrm{d}\tau_\nu} = I_\nu - \int p_\nu I_\nu \frac{\mathrm{d}\Omega}{4\pi} \tag{3}$$

where I_ν is the specific intensity at frequency ν and at optical depth τ_ν below the surface, p_ν is the scattering phase function, and θ is the angle between the direction of propagation and outward surface normal. The phase function, p, is expanded using Legendre polynomials, and to make the case simple, the number of terms in the Legendre polynomials is truncated after the first term. This truncation may result in modeling error [*Pitman et al.*, 2005]; however, as mentioned before, we are interested in the simplest case directly following past works.

Conel [1969] proposed a "cloudy atmosphere" model where a condensed powdered mineral is assumed to be composed of "semi-infinite cloudy atmospheres" in which individual particles scatter and absorb light. This assumption is not strictly true for planetary regolith, in which the particles are in contact; however, it allows a convenient calculation of emissivity using scattering properties from Mie theory. *Conel* [1969] accounts for multiple scattering that happens for closely packed particles using RT theory. Mie theory provides the extinction coefficient (Q_{ext}), scattering coefficient (Q_{sca}), and asymmetry parameter (g), which are the necessary scattering parameters that are used by RT theory to ultimately calculate emissivity.

The two-stream approximation is used to solve equation (3). After solving a set of equations from this method, emissivity is derived as

$$\varepsilon = \frac{2}{u+1} \tag{4}$$

where u is the square root of

$$u^2 = \left(1 - \omega_0 \frac{\omega_1{}'}{3}\right)(1-\omega_0)^{-1} \tag{5}$$

The single scattering albedo, ω_0, is calculated using scattering and extinction efficiencies from the Mie or T-matrix methods as

$$\omega_0 = \frac{Q_{sca}}{Q_{ext}} \tag{6}$$

The Legendre expansion coefficient, $\omega_1^{'}$, can be calculated from cosine asymmetry parameter, g, as $\omega_1^{'} = (2l+1)g^l$ where $l=1$ for Conel's case. The asymmetry parameter is a measure of the amount of radiation scattered into the forward or backward hemisphere [*van de Hulst*, 1957].

2.3.2. Hapke Models

Hapke [1993] and *Hapke* [1996a] also devised RT models for particulate surfaces appropriate for planetary settings. In these models, a heat conduction equation is coupled with the equation of radiative transfer for the visible and thermal infrared. The three fundamental equations to be solved are equations (4), (6), and (7) in *Hapke* [1996a], which correspond to visible RT, thermal RT, and heat conduction, respectively.

The two-stream approximation is used to solve the system of equations, then *Hapke* [1996a] (slightly different but also available in *Hapke* [2012]) derives the solution in two ways. The first is a condition in which a particulate sample is lying on a plate that is being held at a constant temperature and radiating into space from its upper surface. This represents a laboratory setting where the samples are contained in sample holders and heated from below. Here, emissivity is derived as

$$\varepsilon_h = 2\gamma_T/(\zeta_T + \gamma_T) \tag{7}$$

Anisotropic scattering is included with the term ζ_T where $\zeta_T = (1-\beta_T\omega_T)^{1/2}$ and β_T is the hemispherical asymmetry parameter (refer to *Hapke* [1993, 1996a, 2012] for term definitions).

The second case, first derived in *Hapke* [1993], is for particles heated from above by visible radiation. Here absorption and emission of light take place at the surface of a particulate medium, and the visible light absorbed equals power radiated. This gives emissivity as

$$\varepsilon_h(\omega_T) \cong \frac{2\gamma_T}{1+\gamma_T}\left(1 + \frac{1}{6}\frac{1-\gamma_T}{1+\gamma_T}\right) \tag{8}$$

Scattering in equation (8) is assumed to be isotropic; thus, the ζ_T term is absent. In our study, results based on *Hapke* [1993], which does not incorporate the most applicable assumptions to our laboratory setting, are still included as a contrast to *Conel* [1969] and *Hapke* [1996a] models as the *Hapke* [1993] model has been investigated more thoroughly before (e.g., *Moersch and Christensen* [1995], *Pitman et al.* [2005]). With the contrast, the importance of incorporating correct model assumptions is highlighted, particularly with the discussions of the conceptual parameter corrections to the *Hapke* [1993] model that has been frequently used [*Moersch and Christensen*, 1995; *Mustard and Hays*, 1997; *Pitman et al.*, 2005] to produce reasonable spectra and an insight into the similarities of the *Conel* [1969] model to *Hapke* [1993] model caused by a misrepresentation of the asymmetry parameter in *Moersch and Christensen* [1995] and *Cheng et al.* [2010].

γ_T and ζ_T are dependent on single scattering albedo (ω_T) and hemispherical asymmetry parameter (β_T). For ease of calculation, the asymmetry parameter β_T can be substituted with the cosine asymmetry parameter, g, derived from either the Mie or T-matrix model [*Arnold*, 2014; *Glotch et al.*, 2016; *Hardgrove et al.*, 2016].

Table 1. Summary of Six Types of Hybrid Models Studied in This Work[a]

	Conel [1969]	*Hapke* [1993]	*Hapke* [1996a]
T-matrix	T/Conel	T/Hapke93	T/Hapke96
Mie	Mie/Conel	Mie/Hapke93	Mie/Hapke96

[a]*Conel* [1969], *Hapke* [1993], and *Hapke* [1996a] are RT models. T-matrix and Mie methods provide necessary inputs for these RT models to compute emissivity.

In all, this study compares three RT models and two light scattering methods to compute scattering parameters used in these RT models. Theories used in this work are summarized in Table 1, and the names of the six hybrid models will be referred as presented in this table for the remainder of this work.

3. Methods

3.1. Experimental Methods

Both the Mie and T-matrix methods require wavelength-dependent optical constants, *n* and *k*, of minerals. We use the optical constants of enstatite, calculated by *Rucks and Glotch* [2014] for this study (Figure 1). This is a crucial step as previous studies suspected that errors between computational and laboratory spectra are due to discrepancies in optical constants [*Moersch and Christensen*, 1995*; Mustard and Hays*, 1997]. *Rucks and Glotch* [2014] calculated the optical constants of enstatite using the methods of *Arnold et al.* [2014]. The contributions of each of the three principal indices of refraction of enstatite to the emissivity (hemispherical) spectrum of a particulate mixture were calculated by first measuring the spectrum of coarsely ground enstatite (>500 μm) and then inputting that spectrum into a linear retrieval algorithm [*Ramsey and Christensen*, 1998*; Rogers and Aharonson*, 2008] with synthetic oriented enstatite spectra calculated using Fresnel equations (converted to emissivity according to Kirchoff's Law) [*Glotch et al.*, 2006] from the optical constants used

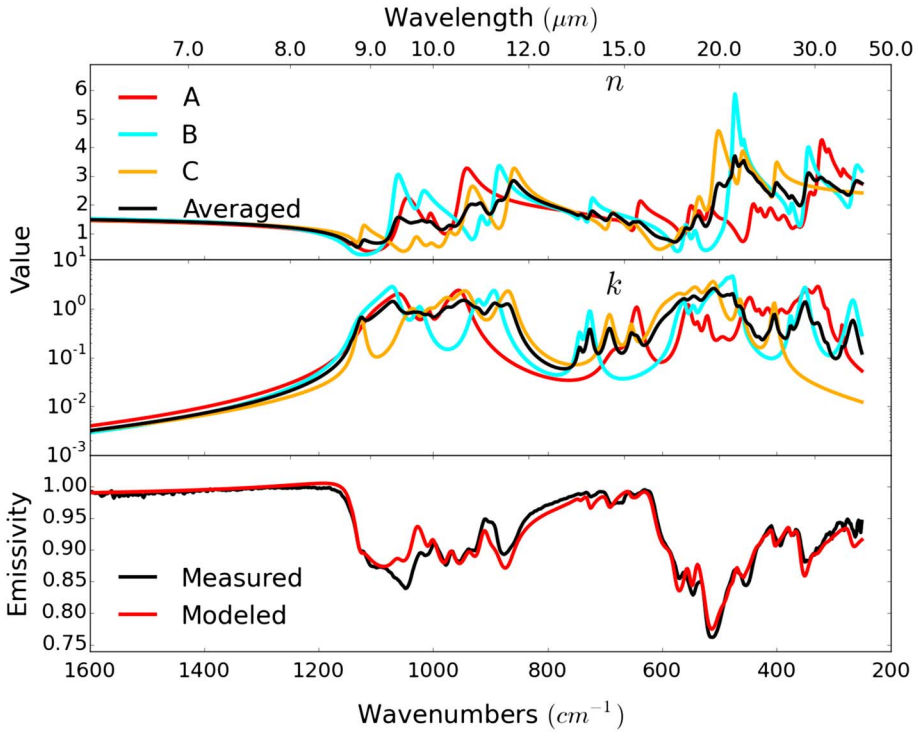

Figure 1. Optical constants (top) *n* and (middle) *k* from *Rucks and Glotch* [2014]. Average is based on 14.7%, 37.3%, and 48.0% weights for *a*, *b*, and *c* principle index of refraction, respectively. (bottom) Measured and modeled spectra of real enstatite particles >500 μm that were used to derive contribution percentages. Modeled spectrum is based on linear mixing algorithm, which is appropriate for large particle sizes compared to the wavelength of light [*Ramsey and Christensen*, 1998].

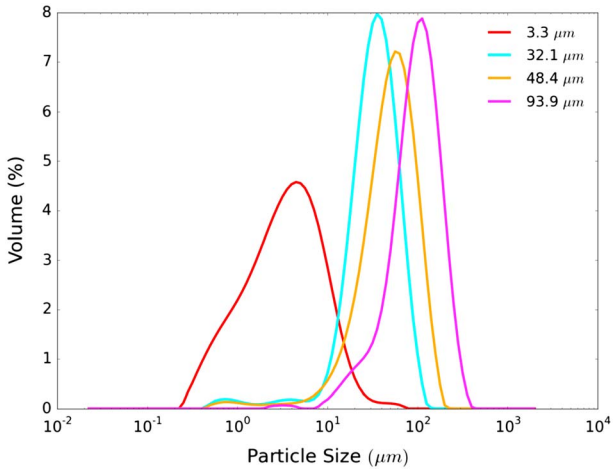

Figure 2. Particle diameter size distribution of enstatite used to obtain laboratory emissivity spectra. Median diameters from these distributions are used for modeling particles in the computational part of this work. Legend is based on the median particle size for each size range.

as the library spectra. This yielded contributions of 14.7%, 37.3%, and 48.0% for principal indices *a*, *b*, and *c*, respectively. As can be seen in Figure 1, the measured emissivity spectrum is fit well (root mean square error of 0.0135), except for a region between ~1000 and 1100 cm^{-1}, where there is a substantial misfit that may be attributed to the exclusion of particle orientation in simplified Fresnel equations for normal incidence angle.

Emissivity (hemispherical) spectra were measured using a Nicolet 6700 Fourier transform infrared spectrometer in the Stony Brook University Center for Planetary Exploration and calibrated employing the methods of *Ruff et al.* [1997].

The same enstatite sample that was used to retrieve the oriented optical constants was ground into finer particle sizes using a mortar and pestle and dry sieved to obtain particle size separates with median diameters of 32.1, 48.4, and 93.9 μm. Additionally, the finest particle size, with a median diameter of 3.3 μm, was separated using Stokes' settling method [*Salemi et al.*, 2010]. Particulate samples were washed to remove clinging fines, then actual particle size distributions were measured using a Malvern Mastersizer 2000 laser diffractometer available in the Department of Geosciences at Stony Brook University (Figure 2). This study requires an accurate knowledge of particle sizes; therefore, we followed high precision techniques presented in *Sperazza et al.* [2004] who were able to accurately measure very fine particles (<10 μm) with a precision of ~5% at two standard deviations.

3.2. Computational Methods

The T-matrix method requires optical constants of minerals as inputs and, additionally, positions of spheres in a cluster and size parameters at every wavelength of interest. The size parameter is the ratio of particle radius to wavelength, expressed as $X = 2\pi r/\lambda$ where r and λ are particle radius and wavelength of observed light, respectively. To generate a cluster of spheres that represents a section of a particulate surface, a collision-driven molecular dynamics algorithm was used [*Donev et al.*, 2005]. This provides *x*, *y*, and *z* coordinates for a specified number of spheres and packing density as well as the diameter of spheres. The limit for the number of spheres in a cluster is dependent on the computational power available to solve the T-matrix equations. Here, we used a cluster of 1000 spheres for the three larger particles sizes. Packing density was set to~0.6, which is close to the limit for close random packing, allowing near maximal chance of multiple scattering that is of importance in this study. For the finest size fraction, we varied the cluster size, using 150, 1000, 5000, and 10,000 particles in order to determine the effects of cluster size on our calculated spectra. We also modeled with lower cluster packing densities of ~0.2 and ~0.4 to examine packing density effects on our modeled spectra. These inputs are required to run the Multiple Sphere T-Matrix (MSTM) code, made publicly accessible by Daniel Mackowski [www.eng.auburn.edu/users/dmckwski/scatcodes] [*Mackowski and Mishchenko*, 2011a, 2011b]. We ran the MSTM code for frequencies within a range of 200 to 1600 cm^{-1} in intervals of 10 cm^{-1} on the NASA Pleiades supercomputer located at NASA Ames Research Center.

The MSTM outputs necessary for our purposes are Q_{ext}, Q_{sca}, and g of the whole cluster. These three parameters were also obtained from Mie calculations for a complementary set of models. We used a MATLAB program provided by *Mätzler* [2002], which is a translation of the Mie scattering coefficient calculation FORTRAN code given in *Bohren and Huffman* [1983]. As with MSTM, the inputs for Mie calculations are optical constants and size parameters.

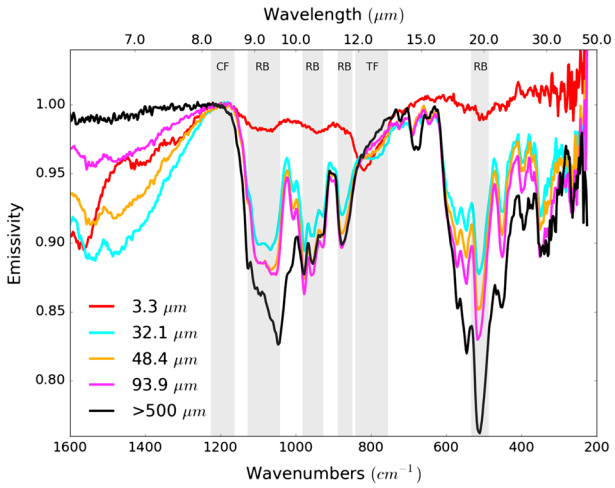

Figure 3. Emissivity spectra of enstatite in five different particle size fractions measured in laboratory. Major Reststrahlen bands (RB) are present between ~850 and 1150 cm^{-1} and at ~500 cm^{-1}. Christiansen feature and transparency feature are observed at ~1200 $cm^{-1}$and ~800 cm^{-1}, respectively. Emissivity values are averages of three sets of laboratory measurements, each consisting of 256 scans.

As a final step, the outputs from the Mie or MSTM models (Q_{ext}, Q_{sca}, and g) are used to compute scattering parameters that are input into emissivity equations based on the Conel (equation (4)) and the two Hapke RT models (equations (7) and (8)) described above. All computationally derived emissivity spectra are compared to spectra acquired in the laboratory.

4. Results

4.1. Experimental Results

Laboratory emissivity measurements of enstatite particles are illustrated in Figure 3. Overall, spectral contrast decreases as particle size decreases.

Several prominent features are present that capture the effect of particle size on emissivity spectra. First, the Christiansen feature, a maximum in emissivity and an indication of change from volume to surface scattering with increasing wavelength, appears at ~1200 cm^{-1}. This occurs

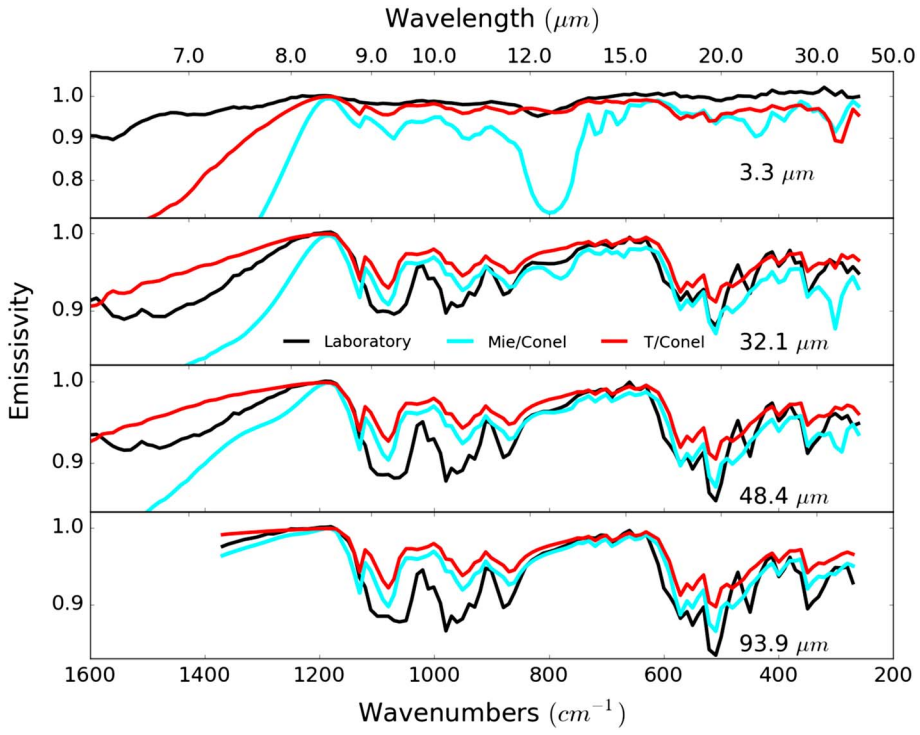

Figure 4. Emissivity spectra of enstatite computed from T/Conel and Mie/Conel hybrid models. Laboratory measurements of real particles are included for comparison. Mie/Conel and laboratory spectral resolution has been adjusted to that of T/Conel spectra. Particle size fractions are 3.3, 32.1, 48.4, and 93.9 μm from top to bottom. The T/Conel model for 3.3 μm size fraction is based on 5000 particles whereas the rest of the size fractions use 1000 particles in clusters during computation. Diffraction subtraction correction has no net effect and is not used. Emissivity at higher frequencies for the 93.9 μm size fraction was not computed to conserve computing resources.

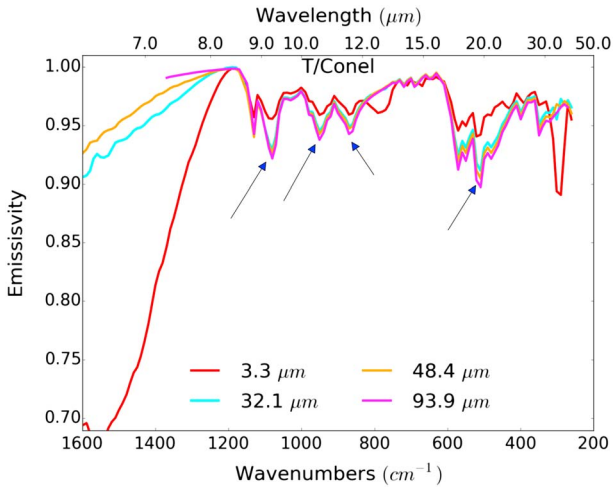

Figure 5. Emissivity spectra from the T/Conel model emphasizing the effect of particle size. Arrows point to Reststrahlen bands where the change in band depth is difficult to model. The depth of the transparency feature at ~800 cm^{-1} is modeled well for 3.3 μm size fraction. Emissivity at high frequencies for the 93.9 μm size fraction was not computed to conserve computing resources.

at the wavelength where the imaginary index of refraction, *k*, is at a minimum, and where the real index of refraction, *n*, equals 1.

Major Reststrahlen bands are observed between ~850 and 1150 cm^{-1} and at ~500 cm^{-1}. Reststrahlen bands are caused by the fundamental vibrational modes of mineral crystal lattices and happen at wavelengths where *k* is large. These features gradually decrease in strength as the median particle size decreases from 93.9 to 48.4 to 32.1 μm and become very weak at 3.3 μm. However, the decrease is not linear, and especially, the differences between 32.1 and 48.4 μm size fractions are sometimes insignificantly small.

For the smallest particle size fraction, a prominent transparency feature is seen at ~800 cm^{-1}. This feature is also noticeable in the 32.1 μm spectrum and less so for the 48.4 μm particle size fractions. It is very weak for the 93.9 μm size fraction spectrum. This transparency feature occurs where *n* and *k* are relatively high and low, respectively.

4.2. Computational Results

4.2.1. Conel Hybrid Models

Spectra of the finest particles (3.3 μm) between ~400 and 1300 cm^{-1} are modeled well by the T/Conel model, particularly compared against the Mie/Conel model. For the 3.3 μm size fraction (Figure 4), a reduction in the strengths of the Reststrahlen bands (at ~850–1150 cm^{-1} and ~500 cm^{-1}) and the presence of a transparency feature (~800 cm^{-1}) are observed when compared to Mie/Conel model. However, the band center of the transparency feature is at a slightly lower frequency than observed in the laboratory spectrum. The T/Conel model does not produce the overamplified spectral contrast seen in the Mie/Conel model for this size fraction except at low frequencies. For example, the transparency feature at ~800 cm^{-1} is not as grossly overestimated for the T/Conel model compared to Mie/Conel model (Figure 4). In addition, the T/Conel modeled fine particulate "silicate rolloff" seen at wavelengths shorter than the Christiansen feature is closer to the laboratory spectrum than the same feature in the Mie/Conel model.

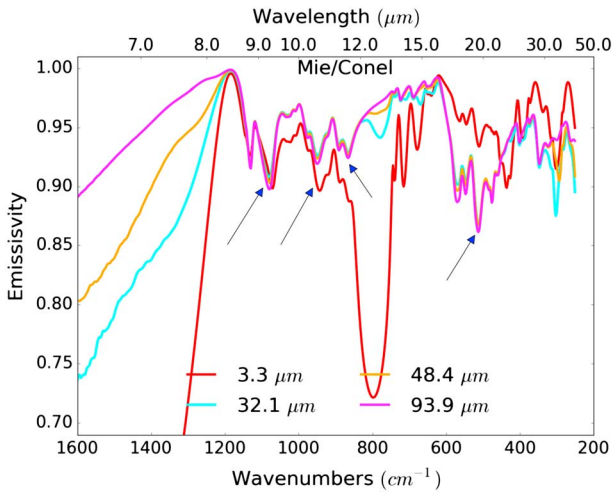

Figure 6. Emissivity spectra calculated using the Mie/Conel hybrid model, emphasizing the effects of particle size. Arrows point to Reststrahlen bands. The depth of the transparency feature at ~800 cm^{-1} is greatly overestimated for the 3.3 μm size fraction.

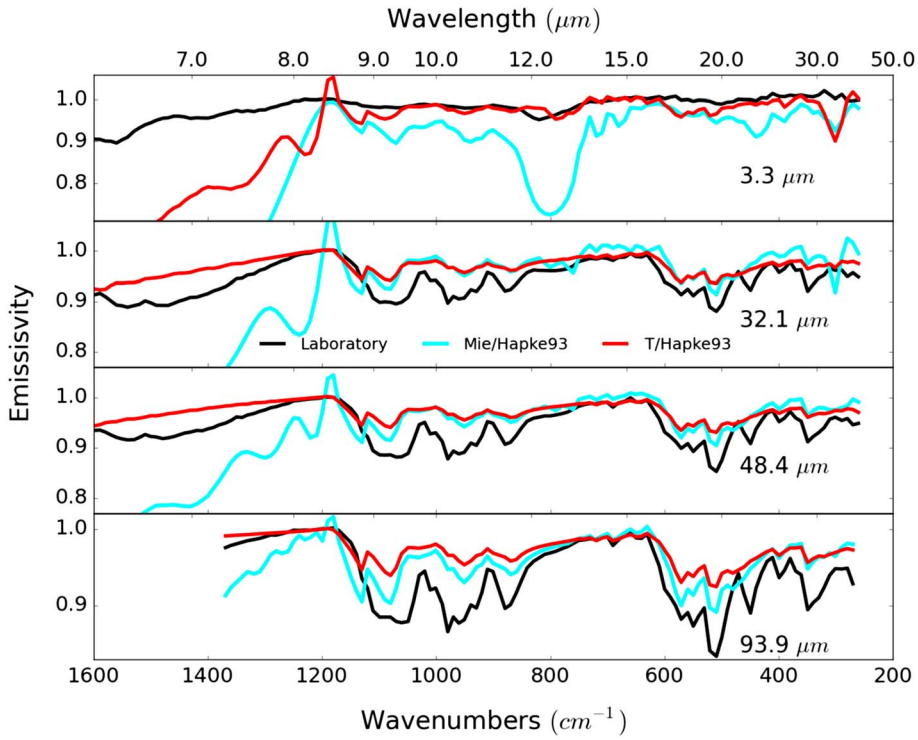

Figure 7. Emissivity spectra of enstatite computed from T/Hapke93 and Mie/Hapke93 hybrid models along with laboratory measurements of real particles. Both Mie/Hapke93 and laboratory spectral resolution has been adjusted to that of T/Hapke93 spectra. Diffraction subtraction correction is used for all modeled spectra except the Mie/Hapke93 3.3 μm size fraction. T/Hapke93 model for 3.3 μm size fraction uses 5000 particles whereas the other size fractions use 1000 particles. Emissivity at high frequencies for the 93.9 μm size fraction was not computed to conserve computing resources.

For larger particle size fractions, the capability of the T/Conel model declines. The shapes of spectra change only slightly as the size fraction increases from 32.1 to 48.4 to 93.9 μm (Figure 5). Although Reststrahlen bands are present in each of these three particle size ranges, band depths do not change considerably. The Mie/Conel model starts to perform equally good as, or even better than, the T/Conel model as particle size increases. However, analogous to the T/Conel model, the shape of spectra for the Mie/Conel model does not change substantially with changing particle size (Figure 6). Both T-matrix and Mie approaches almost equally have difficulty in producing particle size effects for the 32.1 to 93.9 μm size fraction range. Still, it is important to keep in mind that when evaluating the modeled spectra in this way, a clearly substantial decrease in band depths is not necessarily sought after as, already mentioned, even the laboratory spectra do not always exhibit a clear linear trend in the change of band depths.

4.2.2. Hapke Hybrid Models

In general, the Hapke hybrid models follow the same trend observed for Conel hybrid models (Figures 7 and 8). T-matrix-based modeled spectra are more consistent with the laboratory spectra for the finest particle size fraction, but the agreement decreases as particle size increases, and compared to the Mie based models, the agreement at short frequencies is better than that in the 1000 cm^{-1} region. This is consistent with the quality of the laboratory spectrum and modeled spectral fit of coarse particulates (Figure 1).

The T/Hapke96 model generally is in better agreement with the laboratory spectra than the T/Hapke93 model. This is consistent with *Arnold* [2014], who observed that the T/Hapke96 hybrid model is the better performing model based on a study of amorphous silica particles. This is also consistent with the model assumptions. *Hapke* [1993] assumes light incident to a sample from above and isotropic scattering, but *Hapke* [1996a] assumes no incident light, sample heating from below, and anisotropic scattering. In the laboratory setting, samples are heated from below with no incident radiation from above, and perfect isotropic scattering is not achieved. This condition better corresponds to assumptions of *Hapke* [1996a].

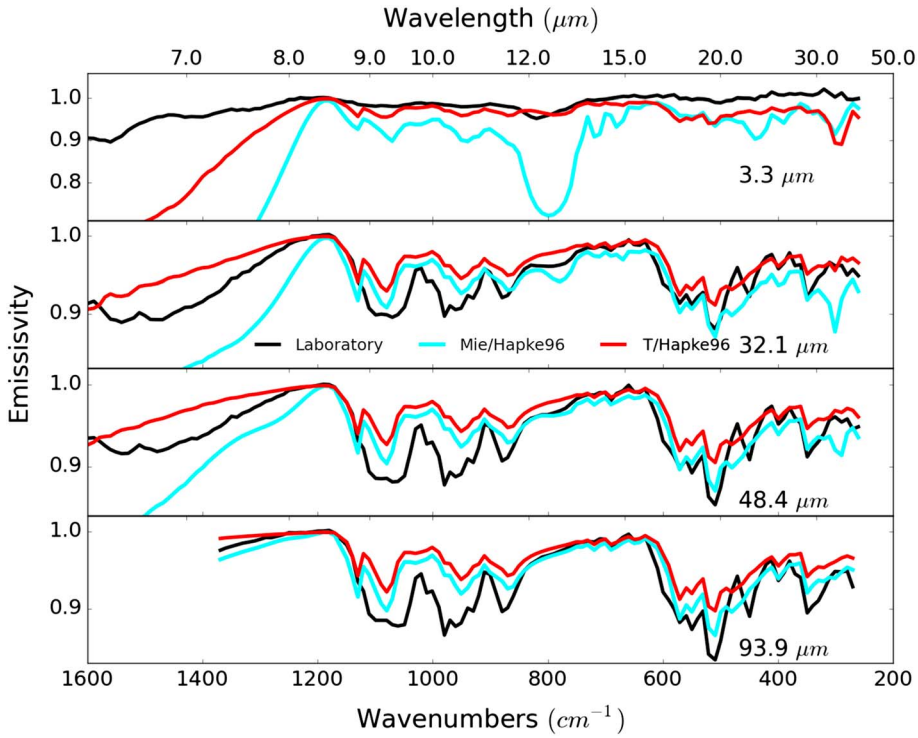

Figure 8. Emissivity spectra of enstatite computed from T/Hapke96 and Mie/Hapke96 hybrid models along with laboratory measurements of real particles. Diffraction subtraction correction has no net effect and is not used.

5. Discussions

5.1. Parameter Correction

The T/Hapke93 and Mie/Hapke93 models require parameter corrections to produce reasonable spectra for all size fractions except for the 3.3 μm Mie/Hapke93 model. When using Mie and RT hybrid models for closely packed large particles, parameters from Mie theory typically need to be corrected for packing effects before employing them to emissivity calculations [*Mishchenko*, 1994; *Wald*, 1994; *Moersch and Christensen*, 1995; *Wald and Salisbury*, 1995; *Mustard and Hays*, 1997; *Pitman et al.*, 2005; *Cheng et al.*, 2010; *Arnold*, 2014]. This is because for particles that are large compared to the wavelength of light, forward scattered light becomes indistinguishable from unscattered light and extinction efficiency of a particle approaches 2, but extinction efficiency cannot be greater than 1 in closely packed particles [*Hapke*, 1981, 1993; *Wald*, 1994]. Mie theory does not take this into account as it was originally intended for isolated particles; therefore, parameters obtained from Mie calculations are corrected when appropriate in this study. The T-matrix method, which is capable of handling closely packed particles, still required parameter correction in our case. The diffraction subtraction correction [*Wald*, 1994] and the static structure factor correction [*Mishchenko*, 1994] are two methods that can correct for close packing effects. Both had similar effectiveness, consistent with *Pitman et al.* [2005] and *Cheng et al.* [2010], and only the diffraction subtraction correction results are shown in Figure 7 as it is simpler and produced slightly better results.

For Mie/Conel and Mie/Hapke96 hybrid models, the diffraction subtraction correction to the single scattering albedo, $w_{\text{diff}} = 2w_{\text{ori}} - 1$, and to the asymmetry parameter, $g_{\text{diff}} = (2w_{\text{ori}}g_{\text{ori}} - 1)/(2w_{\text{ori}} - 1)$, cancel each other out, and the correction has no net effect on emissivity (subscripts "ori" and "diff" indicate original and diffraction subtraction correction terms, respectively).

5.2. Model Comparison

In past works [e.g., *Moersch and Christensen* [1995], *Cheng et al.* [2010], and *Arnold et al.*, 2014] the term u in Conel's RT model is expressed as

$$u^2 = \left(1 - \omega_0 \frac{g}{3}\right)(1 - \omega_0)^{-1} \tag{9}$$

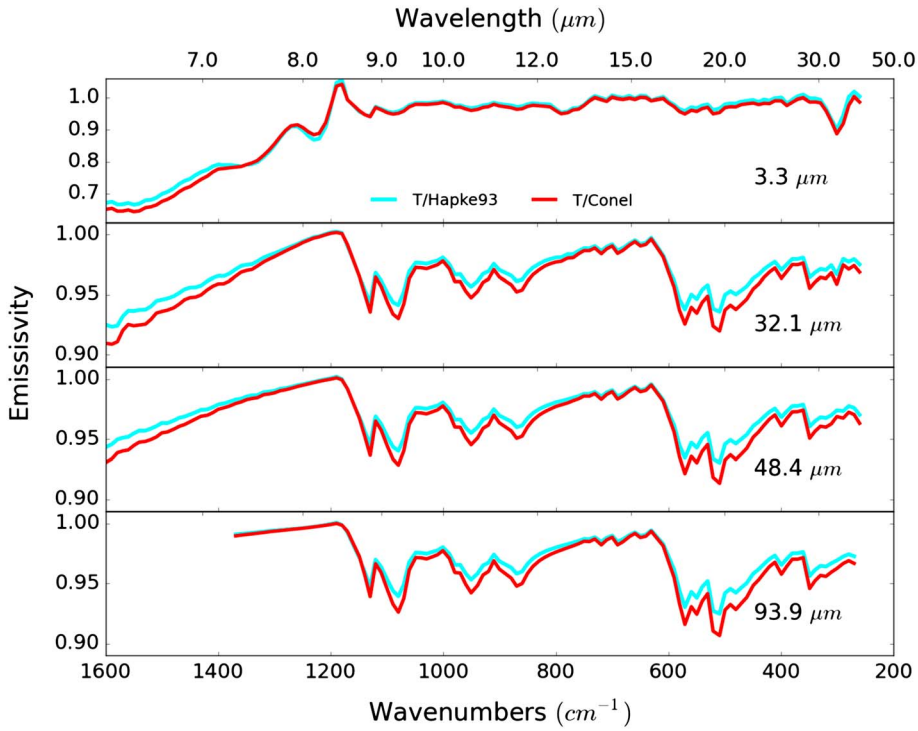

Figure 9. Emissivity spectra from the T/Conel and T/Hapke93 hybrid models highlighting the small difference between the two RT models with $g = \omega_1'$. T/Conel and T/Hapke93 models for 3.3 μm size fraction uses 5000 particles whereas the other size fractions use 1000 particles. Emissivity at high frequencies for the 93.9 μm size fraction was not computed to conserve computing resources.

where the asymmetry parameter is interpreted as $g = \omega_1'$. This results in emissivity spectra shown in Figures 9 and 10. Parameter correction is necessary to produce fair spectra with reasonable emissivity values when the asymmetry parameter is interpreted this way. In this case, spectra of the Conel and the Hapke93 hybrid models are extremely similar to one another.

Nonetheless, *Conel* [1969] originally stated that the asymmetry parameter is defined as $g = \omega_1'/3$. Substituting this into equation (5),

$$u^2 = (1 - \omega_0 g)(1 - \omega_0)^{-1} \tag{10}$$

when u from equation (10) is substituted into equation (4), emissivity, in terms of single scattering albedo and asymmetry parameter, is written as

$$\varepsilon = \frac{2(1 - \omega_0)^{(1/2)}}{(1 - \omega_0 g)^{(1/2)} + (1 - \omega_0)^{(1/2)}} \tag{11}$$

Equation (11) is comparable to the emissivity expression from *Hapke* [1996a], $\varepsilon_h = 2\gamma_T/(\zeta_T + \gamma_T)$ (equation (7)) once the definitions of γ and ζ, $\gamma = (1 - \omega_0)^{(1/2)}$ and $\zeta = (1 - \beta\omega_0)^{(1/2)}$, are utilized (subscript T for thermal infrared wavelengths are dropped). Equation (7) expression becomes

$$\varepsilon_h = \frac{2(1 - \omega_0)^{(1/2)}}{(1 - \omega_0 \beta)^{(1/2)} + (1 - \omega_0)^{(1/2)}} \tag{12}$$

When the asymmetry parameter is defined as $\beta = g$, equations (11) and (12) become identical, meaning that RT model of *Conel* [1969] and *Hapke* [1996a] are equivalent under these conditions. This is plausible as *Conel* [1969] considered an alternative method of arriving at his emissivity equation by instead considering the case of a thermally emitting semi-infinite cloud with zero incident external radiation with local thermodynamic

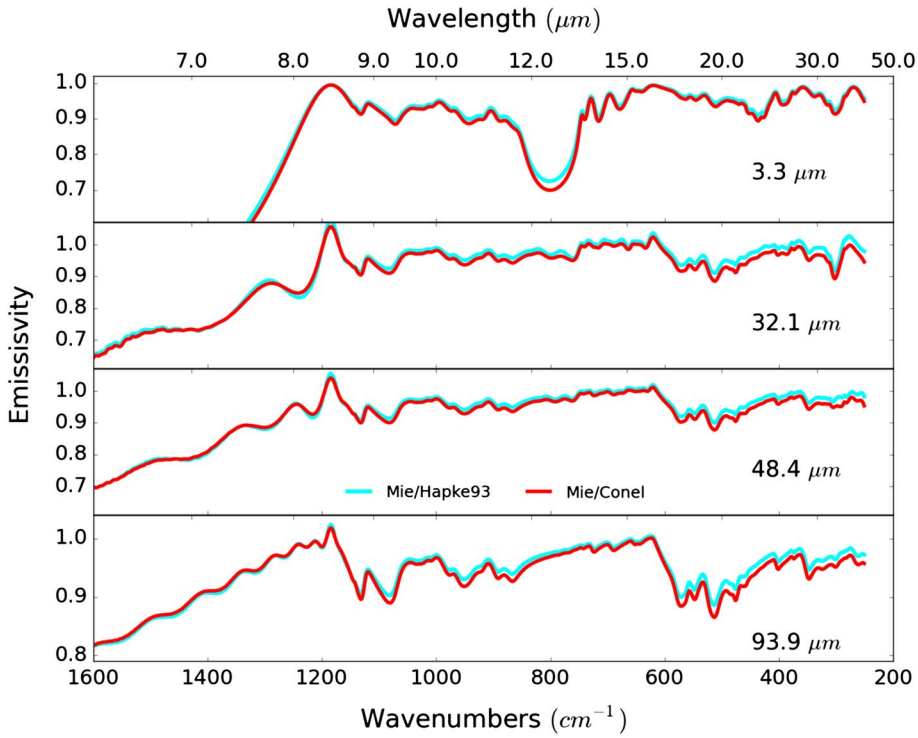

Figure 10. Emissivity spectra from the Mie/Conel and Mie/Hapke93 hybrid models highlighting the small difference between the two RT models with $g = \omega_1'$.

equilibrium. This alternative approach corresponds with assumptions taken by *Hapke* [1996a] where he considered a sample heated from below with no incident radiation from above. Emissivity spectra, therefore, for the Conel and Hapke96 hybrid models are identical (Figures 4 and 8) for the set of assumptions we used. In this manner, parameter correction is not necessary for the Conel hybrid models to produce reasonable spectra. Furthermore, the agreement between laboratory and modeled spectra is better for the Conel hybrid models than Hapke93 hybrid models.

5.3. Modeling Difficulties

5.3.1. Low Frequency Region (200–300 cm^{-1})

Some errors for the T-matrix hybrid models are observed in portions of the low wavenumber (200–300 cm^{-1}, 33.3–50 μm) region (Figures 4, 7, and 8). The performance in this region is likely affected by the size of clusters. For 3.3 μm size fraction, the errors between laboratory and T-matrix hybrid models are large because the cluster diameter, approximately 40 μm with 1000 particles, is on the order of the wavelength of light (~30–50 μm). Here, the whole cluster diffracts light as if it was a Mie single scattering particle with diameter of 40 μm, and the scattering properties are influenced by this single scattering behavior of the cluster. The 32.1, 48.4, and 93.9 μm size fraction clusters composed of 1000 particles have cluster diameters 380, 575, and 1110 μm, respectively, which are large compared to the wavelength in this region. For these larger particle sizes, clusters do not diffract light as much, and the over-reduction in emissivity observable in the 3.3 μm size fraction is not present (Figures 4, 7, and 8). For this reason, the cluster size of 3.3 μm size fraction was changed to include as many as 5000 and 10,000 spheres, which gives a cluster diameter of 67 and 85 μm, respectively (Figures 11 and 12). Still larger clusters are desirable, but the computational burden grows roughly as the cube of the cluster size.

Mie hybrid models do not contain clusters as in T-matrix hybrid models, yet similar errors at low wavenumbers are observed when particle size is on the order of observed light. This is illustrated by 32.1 and 48.4 μm size fractions. Calculated emissivity is unnaturally low for these size fractions. The 93.9 μm particle size fraction however compares reasonably well with the laboratory spectrum at low wavenumbers because the particle size is adequately larger than the wavelength of light (Figures 4, 7, and 8).

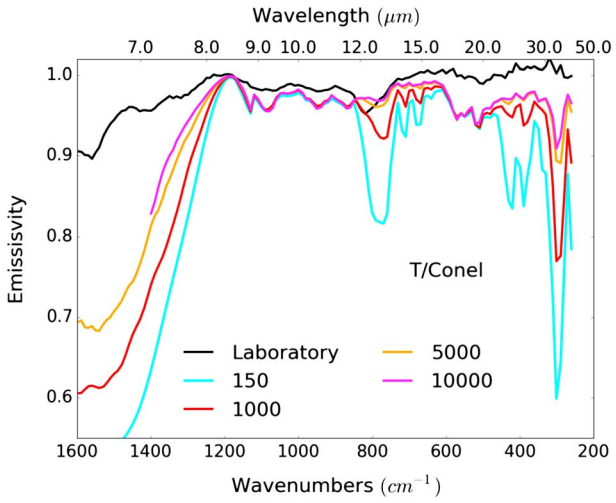

Figure 11. Emissivity spectra of 3.3 μm size fraction from T/Conel model showing the effect of changing the number of particles in a cluster during T-matrix computation. The laboratory measurement of the 3.3 μm size fraction is included as a reference. Modeled spectra approach the laboratory spectrum as the number of particles increases. Cluster diameters are 20, 40, 67, and 85 μm for 150, 1000, 5000, and 10,000 particle clusters, respectively. Emissivity at high frequencies for the 10,000 particle cluster was not computed to conserve computing resources.

5.3.2. High Frequency Region (1300–1600 cm^{-1})

Portions of the high frequency region (1300–1600 cm^{-1}, 6.25–7.7 μm) also show errors for both T-matrix and Mie hybrid models, especially for the 3.3 μm size fraction (Figures 4, 7, and 8). Diffraction is once again likely playing a role in modeling difficulty. In the T-matrix hybrid models, the size of individual particles (3.3 μm) is on the order of the wavelength of light (~6–8 μm). Single scattering albedo increases due to an increase in scattering cross section with diffraction, which consequently decreases emissivity. For larger size fractions, emissivity remains high and relatively close to laboratory measurements. A possible cause of this discrepancy in the T-matrix hybrid models for the finest size fraction is the number of particles used in the computations. One thousand, and even 10,000, particles might not be enough to produce emissivity spectra consistent with laboratory spectra in this wavenumber range. Compared to the computational particle cluster, a lab sample contains orders of magnitude more mineral particles within the instrument sampling area. Ten thousand particles used in the computation appear to be insufficient to overcome most of the diffraction effects with close packing of particles. As indicated by the pattern in modeling improvement from 150 to 10,000 particle clusters (Figures 11 and 12), modeling errors in T-matrix hybrid models in this region are expected to improve if more particles are used, but for now it is computationally prohibitive to model clusters that have orders of magnitude more particles. The errors of Mie hybrid models at high wavenumbers are also likely influenced by diffraction. As particle size increases, less diffraction occurs and modeling results of Mie hybrid models improve.

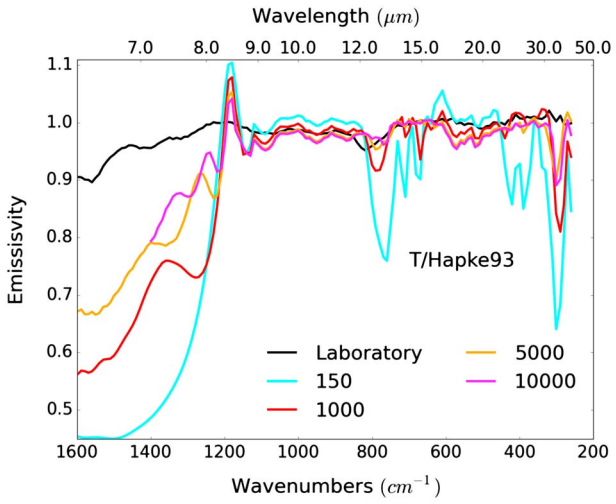

Figure 12. Emissivity spectra of 3.3 μm size fraction from T/Hapke93 model showing the effect of changing the number of particles in a cluster during T-matrix computation. The laboratory measurement of the 3.3 μm size fraction is included as a reference. T/Hapke 96 model is not shown as the spectra produced are equivalent to T/Conel model.

In order to probe the effects of cluster size for a given number of particles, we reduced the packing density of the clusters in the T-matrix hybrid models to see if modeled emissivity in the high wavenumber region could be improved. Spectra from the T/Hapke96 model are plotted in Figure 13 to show the representative trend of all models. As the packing density decreases, the effect of multiple scattering decreases and spectra from the T-matrix hybrid models become more like those of Mie hybrid

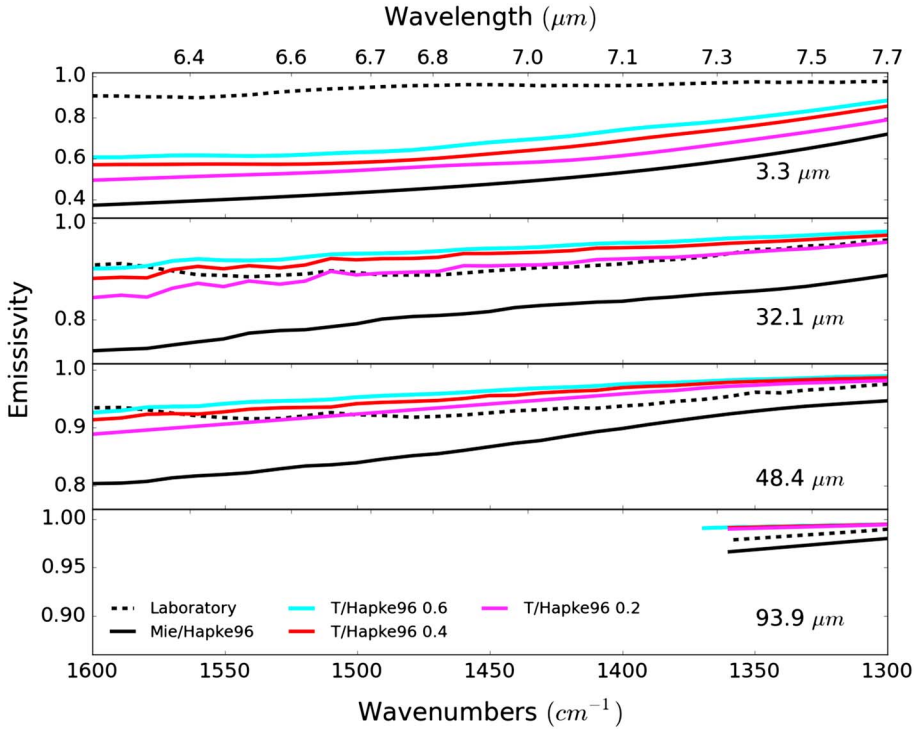

Figure 13. T/Hapke96 hybrid model spectra showing the effect of changing packing density of clusters used in the models. Figure is zoomed in on high wavenumbers 1300–1600 cm^{-1}. One thousand particles were used for clusters at all size fractions. Emissivity at high frequencies for the 93.9 μm size fraction was not computed to conserve computing resources.

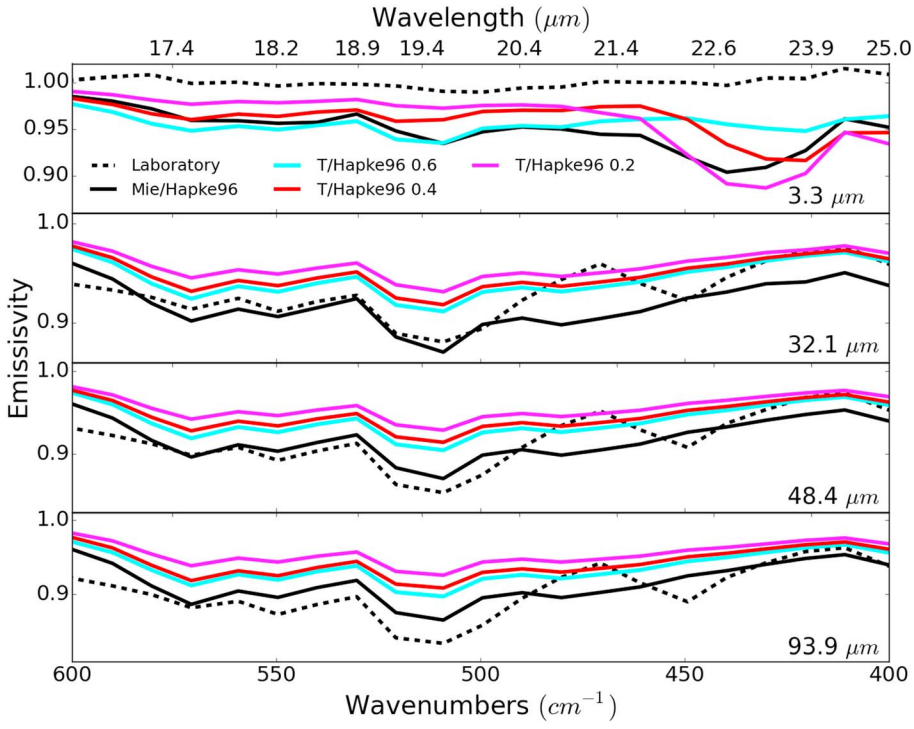

Figure 14. T/Hapke96 hybrid model spectra showing the effect of changing packing density of clusters used in the models. Figure is zoomed in on Reststrahlen band at ~510 cm^{-1}.

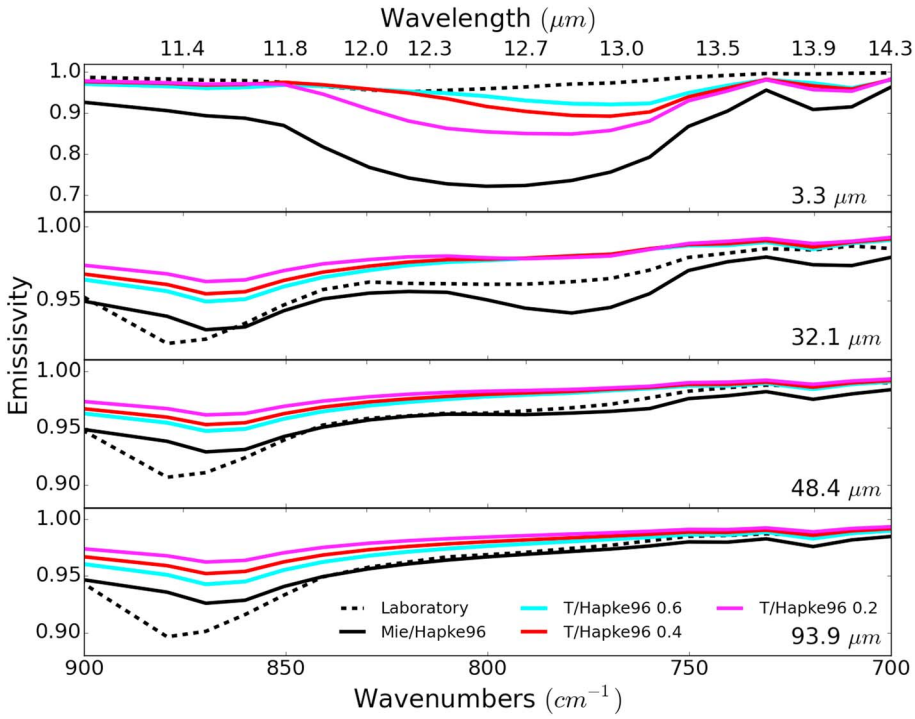

Figure 15. T/Hapke96 hybrid model spectra showing the effect of changing packing density of clusters used in the models. Figure is zoomed in on transparency feature at ~780 cm^{-1}.

models. For the smaller particle size fractions, diffraction contributes to larger single scattering albedos, which are not subdued as much in lower packing density clusters, and consequently, emissivity is lower for lower packing density clusters. As particle size increases, the diffraction effect becomes weaker and emissivity increases. The effect of packing density is relatively weak for the larger particle sizes.

5.3.3. Reststrahlen Bands, Christiansen Features, and Transparency Features

Spectral feature positions can be difficult to model. For instance, the modeled Christiansen feature and Reststrahlen band at 1150 cm^{-1} are located at slightly higher frequencies than the laboratory spectra, whereas the transparency feature is located at a slightly lower frequency. Also, the band depth of Reststrahlen bands is almost always underestimated by the T-matrix hybrid models in size fractions 32.1–93.9 μm. The packing density of the cluster was decreased to 0.4 and 0.2 to see if modeled results improved (Figures 14 and 15). Under these scenarios, the transparency features become more like Mie single scattering behavior, but band depths of Reststrahlen bands decreased as Reststrahlen bands are a surface scattering feature, and the behavior is the opposite of the Mie-like behavior.

These difficulties in modeling band center positions and depths are observed in the Mie hybrid models as well. In the case of Reststrahlen bands, optical constants *n* and/or *k* are high, and past studies (e.g., *Moersch and Christensen* [1995], *Mustard and Hays* [1997], *Pitman et al.* [2005]) have indicated difficulty in modeling based on RT models when *n* and *k* are high. Knowing that these issues are common to both Mie and T-matrix approaches and the relatively noteworthy misfits of modeled mixed spectrum of >500 μm particles (Figure 1), there may be an error in the assignment of oriented optical constant percentages and/or the original data in *Rucks and Glotch* [2014], change in optical constants themselves due to grinding, the use of spherical particles as opposed to more realistic shapes (e.g., *Pitman et al.* [2005]), limits of the applicability of RT theory to densely packed particulate media [*Mackowski*, 2017; *Ramezan pour and Mackowski*, 2017], or some other unknown factor.

6. Conclusions

In the search for a more effective light scattering model for particulate media, we modeled emissivity spectra of enstatite particles at MIR wavelengths using six different hybrid models. The T-matrix approach, in

particular the T/Conel and T/Hapke96 hybrid models, were able to better model emissivity spectra of the finest particle size in the ~400 to ~1300 cm^{-1} range. For this size fraction and frequency range, the three T-matrix hybrid models were generally more consistent with laboratory measurements than the three Mie hybrid models and did not overestimate spectral contrast (e.g., transparency feature) as much as the Mie approach. The effectiveness of T-matrix hybrid models decreased with increasing particle size, but the same trend was also observed in Mie hybrid models which is a likely indication that the cause of the disagreement is attributed to common factors between the two types of hybrid models such as model inputs (enstatite optical constants).

In the T-matrix/RT hybrid models, multiple scattering is incorporated which makes them, unlike Mie/RT hybrid models that are based on single scattering, more realistic models for application to planetary regolith where the particulates are closely packed. This increased fidelity to reality increases the likelihood that such models can be used to determine the compositions of finely particulate surfaces like Martian dusty regions or lunar regolith from MIR spectra. The effectiveness of the T-matrix/RT hybrid models has already allowed researchers to constrain mineral percentages in fine particulate mixtures [*Glotch et al*., 2016]. Mie-based approaches would likely have a tremendous difficulty completing a similar task due to very poor modeling of spectral features (e.g., transparency features, Reststrahlen bands) that make the Mie/RT modeled spectra mostly impractical for such applications. The better agreement of the T-matrix/RT modeled spectra with the laboratory spectra in this work is a demonstration that a more realistic treatment of light scattering in closely packed media with particle size comparable to the wavelength of light can indeed improve modeling quality.

With this foundation, the next logical step is to combine a rigorous light scattering model like the T-matrix method with more rigorous methods to solve RT equation such as the adding-doubling method [*de Haan et al.*, 1987], discrete-ordinates method [*Stamnes et al.*, 1988], and Ambartsumian invariant imbedding solution [*Mishchenko et al*., 1999, 2015]. The advantages of the RT models used here were already noted in section 2.3, but the scope of Hapke and similar models must be understood as their physical meaningfulness is debatable (mostly for reflectance, but also applicable to emission) [*Mishchenko*, 1994; *Hapke*, 1996b; *Mishchenko and Macke*, 1997; *Hapke*, 1999; *Mishchenko et al.*, 1999; *Hapke et al.*, 2009; *Shkuratov et al*., 2012, 2013; *Hapke*, 2013]. Future works will further investigate the T-matrix-based models by including as much physically realistic conditions as possible and should inspire the models' development to applications to remotely sensed data.

Acknowledgments
All data and models presented in the manuscript will be placed on the Stony Brook Academic Commons permanent archive (http://commons.library.stonybrook.edu/). This work was supported by the RIS^{4}E node of NASA's Solar System Exploration Virtual Institute (T.D.G., PI) and NSF award # AST-1150652 (T.D.G., PI).

References

Arnold, J. A., T. D. Glotch, and A. M. Plonka (2014), Mid-infrared optical constants of clinopyroxene and orthoclase derived from oriented single-crystal reflectance spectra, *Am. Mineral.*, *99*, 1942–1955.
Arnold, J. A. (2014), Refining mid-infrared emission spectroscopy as a tool for understanding planetary surface mineralogy through laboratory studies, computational models, and lunar remote sensing data, PhD thesis, Stony Brook Univ., Stony Brook.
Bohren, C. F., and D. R. Huffman (Eds.) (1983), *Absorption and Scattering of Light by Small Particles*, pp. 475–489, Wiley, New York.
Cheng, J., S. Liang, F. Weng, J. Wang, and X. Li (2010), Comparison of radiative transfer models for simulating snow surface thermal infrared emissivity, *IEEE J. Sel. Top. Appl. Earth Obs. Remote Sens.*, *3*(3), 1939–1404.
Conel, J. E. (1969), Infrared emissivities of silicates: Experimental results and a cloudy atmosphere model of spectral emission from condensed particulate mediums, *J. Geophys. Res.*, *74*, 1614–1634, doi:10.1029/JB074i006p01614.
de Haan, J. F., P. B. Bosma, and J. W. Hovenier (1987), The adding method for multiple scattering calculations of polarized light, *Astron. Astrophys.*, *183*, 371–391.
Donev, A., S. Torquato, and F. H. Stillinger (2005), Neighbor list collision-driven molecular dynamics simulation for nonspherical hard particles. I. Algorithmic details, *J. Comput. Phys.*, *202*(2), 737–764, doi:10.1016/j.jcp.2004.08.014.
Glotch, T. D., P. R. Christensen, and T. G. Sharp (2006), Fresnel modeling of hematite crystal surfaces and application to martian hematite spherules, *Icarus*, *181*, 408–4018.
Glotch, T. D., J. L. Bandfield, M. J. Wolff, J. A. Arnold, and C. Che (2016), Constraints on the composition and particle size of chloride salt-bearing deposits on mars, *J. Geophys. Res. Planets*, *121*, 454–471, doi:10.1002/2015JE004921.
Hapke, B. (1981), Bidirectional reflectance spectroscopy: 1. Theory, *J. Geophys. Res.*, *86*, 3039–3054, doi:10.1029/JB086iB04p03039.
Hapke, B. (Ed.) (1993), *Theory of Reflectance and Emittance Spectroscopy*, pp. 358–385, Cambridge Univ. Press, New York.
Hapke, B. (1996a), A model of radiative and conductive energy transfer in planetary regoliths, *J. Geophys. Res.*, *101*, 16,817–16,831, doi:10.1029/96JE00917.
Hapke, B. (1996b), Are planetary regolith particles back scattering? Response to a paper by M. Mishchenko, *J. Quant. Spectrosc. Radiat. Transfer*, *55*(6), 837–848.
Hapke, B. (1999), Scattering and diffraction of light by particles in planetary regoliths, *J. Quant. Spectrosc. Radiat. Transfer*, *61*(5), 565–581.
Hapke, B. (Ed.) (2012), *Theory of Reflectance and Emittance Spectroscopy*, 2nd ed., pp. 412–462, Cambridge Univ. Press, New York.
Hapke, B. (2013), Comment on "A critical assessment of the Hapke photometric model" by Y. Shkuratov et al., *J. Quant. Spectrosc. Radiat. Transfer*, *116*, 184–190.

Hapke, B., M. K. Shepard, R. M. Nelson, W. D. Smythe, and J. L. Piatek (2009), A quantitative test of the ability of models based on the equation of radiative transfer to predict the bidirectional reflectance of a well-characterized medium, *Icarus*, *199*, 210–218.
Hardgrove, D. J., A. D. Rogers, T. D. Glotch, and J. A. Arnold (2016), Thermal emission spectroscopy of microcrystalline sedimentary phases: Effects of natural surface roughness on spectral feature shape, *J. Geophys. Res. Planets*, *121*, 542–555, doi:10.1002/2015JE004919.
Hunt, G. R., and L. M. Logan (1972), Variation of single particle mid-infrared emission spectrum with particle size, *Appl. Opt.*, *11*(1), 142–147.
Mackowski, D. W. (1994), Calculation of total cross sections of multiple-sphere clusters, *J. Opt. Soc. Am. A*, *11*(11), 2851–2861.
Mackowski, D. W. (2017), Van de Hulst essay: The DDA, the RTE, and the computation of scattering by plane parallel layers of particles, *J. Quant. Spectrosc. Radiat. Transfer*, *189*, 43–59.
Mackowski, D. W., and M. I. Mishchenko (1996), Calculation of the T matrix and the scattering matrix for ensembles of spheres, *J. Opt. Soc. Am. A*, *13*(11), 2266–2278.
Mackowski, D. W., and M. I. Mishchenko (2011a), A multiple sphere T-matrix Fortran code for use on parallel computer clusters, *J. Quant. Spectrosc. Radiat. Transfer*, *112*, 2182–2192.
Mackowski, D. W., and M. I. Mishchenko (2011b), Direct simulation of multiple scattering by discrete random media illuminated by Gaussian beams, *Phys. Rev. A*, *83*, 013804.
Mätzler, C. (2002), MATLAB functions for Mie scattering and absorption, Research Report 2002-11, Universitas Bernensis, Institut fu¨r Angewandte Physik, Bern, Schweiz.
Mishchenko, M. I. (1994), Asymmetry parameters of the phase function for densely packed scattering grains, *J. Quant. Spectrosc. Radiat. Transfer*, *52*(1), 95–110.
Mishchenko, M. I. (2008), Multiple scattering, radiative transfer, and weak localization in discrete random media: Unified microphysical approach, *Rev. Geophys.*, *46*, RG2003, doi:10.1029/2007RG000230.
Mishchenko, M. I., and A. Macke (1997), Asymmetry parameters of the phase function for isolated and densely packed spherical particles with multiple internal inclusions in the geometric optics limit, *J. Quant. Spectrosc. Radiat. Transfer*, *57*(6), 767–794.
Mishchenko, M. I., and P. A. Martin (2013), Peter Waterman and T-matrix methods, *J. Quant. Spectrosc. Radiat. Transfer*, *123*, 2–7.
Mishchenko, M. I., J. M. Dlugach, D. G. Yanovitskij, and N. T. Zakharova (1999), Bidirectional reflectance of flat, optically thick particulate layers: An efficient radiative transfer solution and applications to snow and soil surfaces, *J. Quant. Spectrosc. Radiat. Transfer*, *63*, 409–432.
Mishchenko, M. I., J. M. Dlugach, J. Chowdhary, and N. T. Zakharova (2015), Polarized bidirectional reflectance of optically thick sparse particulate layers: An efficient numerically exact radiative-transfer solution, *J. Quant. Spectrosc. Radiat. Transfer*, *156*, 97–108.
Moersch, J. E., and P. R. Christensen (1995), Thermal emission from particulate surfaces: A comparison of scattering models with measured spectra, *J. Geophys. Res.*, *100*(E4), 7465–7477, doi:10.1029/94JE03330.
Mustard, J. F., and J. E. Hays (1997), Effects of hyperfine particles on reflectance spectra from 0.3 to 25 μm, *Icarus*, *125*, 145–163.
Pitman, K. M., M. J. Wolff, and G. C. Clayton (2005), Application of modern radiative transfer tools to model laboratory quartz emissivity, *J. Geophys. Res.*, *110*, E08003, doi:10.1029/2005JE002428.
Pitman, K. M., M. J. Wolff, E. A. Cloutis, P. Mann, M. Cuddy, D. Applin, and A. Chanou (2015), *n*, *k* for Mars remote sensing and MSTM modeling, *Proc. Lunar and Planet. Sci. Conf. 46th*, 2236 pp., Woodlands, Tex.
Ramezan pour, B., and D. W. Mackowski (2017), Radiative transfer equation and direct simulation prediction of reflection and absorption by particle deposits, *J. Quant. Spectrosc. Radiat. Transfer*, *189*, 361–368.
Ramsey, M. S., and P. R. Christensen (1998), Mineral abundance determination: Quantitative deconvolution of thermal emission spectra, *J. Geophys. Res.*, *103*(B1), 577–596, doi:10.1029/97JB02784.
Rogers, A. D., and O. Aharonson (2008), Mineralogical composition of sands in Meridiani Planum determined from Mars Exploration Rover data and comparison to orbital measurements, *J. Geophys. Res.*, *113*, E06S14, doi:10.1029/2007JE002995.
Rucks, M., and T. D. Glotch (2014), Mid IR optical constants of orthopyroxenes, AGU Fall Meeting, Abstract P23B-3987.
Ruff, W. R., P. R. Christensen, P. W. Parbera, and D. L. Anderson (1997), Quantitative thermal emission spectroscopy of minerals: A laboratory technique for measurement and calibration, *J. Geophys. Res.*, *102*(B7), 14,899–14,913, doi:10.1029/97JB00593.
Salemi, E., U. Tessari, N. Colombani, and M. Mastrocicco (2010), Improved gravitational grain size separation method, *Appl. Clay Sci.*, *48*, 612–614.
Salisbury, J. W., and J. W. Eastes (1985), The effect of particle size and porosity on spectral contrast in the mid-infrared, *Icarus*, *64*(3), 586–588.
Salisbury, J. W., and A. Wald (1992), The role of volume scattering in reducing spectral contrast of Reststrahlen bands in spectra of powdered minerals, *Icarus*, *96*(1), 121–128.
Shkuratov, Y., V. Kaydash, V. Korokhin, Y. Velikodsky, D. Petrov, E. Zubko, D. Stankevich, and G. Videen (2012), A critical assessment of the Hapke photometric model, *J. Quant. Spectrosc. Radiat. Transfer*, *113*, 2431–2456.
Shkuratov, Y., V. Kaydash, V. Korokhin, Y. Velikodsky, D. Petrov, E. Zubko, D. Stankevich, and G. Videen (2013), Response to the comment by B. Hapke on "a critical assessment of the Hapke photometric model", *J. Quant. Spectrosc. Radiat. Transfer*, *116*, 191–195.
Sperazza, M., J. N. Moore, and M. S. Hendrix (2004), High-resolution particle size analysis of naturally occurring very fine-grained sediment through laser diffractometery, *J. Sediment. Res.*, *74*(5), 736–743.
Stamnes, K., S. C. Tsay, W. Wiscombe, and K. Jayaweera (1988), Numerically stable algorithm for discrete-ordinate-method radiative transfer in multiple scattering and emitting layered media, *Appl. Opt.*, *27*(12), 2502–2509.
van de Hulst, H. C. (Ed.) (1957), *Light Scattering by Small Particles*, 470 pp., John Wiley, New York.
Wald, A. E. (1994), Modeling thermal infrared (2–14 μm) reflectance spectra of frost and snow, *J. Geophys. Res.*, *99*(B12), 24,241–24,250, doi:10.1029/94JB01560.
Wald, A. E., and J. W. Salisbury (1995), Thermal infrared directional emissivity of powdered quartz, *J. Geophys. Res.*, *100*(B12), 24,665–24,675, doi:10.1029/95JB02400.
Waterman, P. C. (1969), New formulation of acoustic scattering, *J. Acoust. Soc. Am.*, *45*, 1,417–1,429.